arXiv:cond-mat/0002325v1 [cond-mat.mes-hall] 21 Feb 2000

The theory of GMR and TMR in segmented magnetic nanowires.

M. Ye. Zhuravlev[a,*)], H. O. Lutz[a], A. V. Vedyayev[b,**)]

[a] *Fakultät für Physik, Universität Bielefeld, 33501 Bielefeld 1, Germany*
[b] *CEA/Département de Recherche Fondamentale sur la Matiére Condensée, SP2M/NM, 38054 Grenoble, France*
[*)] *on leave from N. S. Kurnakov Institute of General and Inorganic Chemistry of the RAS, 117907 Moscow, Leninskii prosp., 31, Russia*
[**)] *on leave from Department of Physics, Moscow State University, Moscow, 119899, Russia*

PACS: 73.40. -c; 73.50.Gr; 73.61. -r

We calculate the resistivity and Giant Magnetoresistance (GMR) of a segmented nanowire consisting of two ferromagnetic segments separated by a thin paramagnetic spacer. The quantization of the electron motion due to the small nanowire cross-section is taken into account; $s-d$ electron scattering gives rise to different mean free paths for spin-up and spin-down s-electrons. The calculated resistivity and GMR oscillate as a function of nanowire cross-section due to the difference in Fermi momenta of d-electrons with opposite spins. The GMR can reach values much higher than those which are obtained for "wires" of infinite cross-section (i.e., a multilayer). Similarly we have calculated the Tunneling Magnetoresistance (TMR) by replacing the paramagnetic spacer with an insulator spacer.

Since its discovery, the Giant Magnetoresistance (GMR) effect in magnetic multilayers [1] has attracted considerable attention due to its fundamental interest as well as its application potential (for a recent reference on the subject cf. [2]). In most studies so far the magnetic structures consist of a number of thin layers of very large lateral extension; thus, quantum size effects and the corresponding charge localisation occurs only in the component perpendicular to the layers. It is to be expected, however, that progress in miniaturisation of technical elements will require the understanding of systems whose lateral extension is limited, too. This is the topic of our letter. Specifically, we investigate electron transport perpendicular to the layer structure. In contrast to earlier theoretical studies [3-6] of this CPP geometry (**c**urrent **p**erpendicular to **p**lanes of infinite lateral extension), we treat the electron transport in a segmented nanowire: two ferromagnetic segments are separated by a thin spacer, and charge localisation is thus threedimensional. As a consequence, the GMR oscillates not only as a function of layer thickness, but also as a function of the wire cross section.

In the above-mentioned earlier studies of magnetic multilayers [3-6] the free-electron model has been used taking into account the exchange splitting of the d-bands, yielding different values of the elastic mean free paths for up and down spin s-electrons. More recently, the GMR was calculated employing realistic band structures of the ferromagnetic and paramagnetic metallic layers [7, 8, 9, 10, 11]. One of the main conclusion was the observation that a correct description of the GMR can be achieved if $sp-d$ hybridization is taken into account.

In the present work we extend the quantum theory of the GMR presented e.g. in ref.[5]; it is based on the theory of spin-dependent scattering of conduction electrons as developed in ref.[12], assuming that s-electrons give the main contribution to the current due to their low effective mass [13] . Their mean free path depends on the spin due to $s-d$ hybridization and the different density of states (DOS) of the d-electrons at the Fermi level. Comparable to the treatment of the layers as a random binary alloy, we calculate the mean-free paths in the framework of the coherent potential approximation(CPA), using the main conclusion of [14] in that the effective mean free paths $l^{\uparrow,\downarrow}$ of the s-electrons are proportional to the DOS $\rho_{d\uparrow,\downarrow}$ of the d-electrons (the arrows indicate the spin direction). The conduction electrons are treated as a free electron gas, and the details of the band structure are neglected. We want to point out, however, that in spite of the simplicity of this model we have taken $s-d$ hybridization into account.

The calculations of resistivities and magnetoresistance are performed on the basis of the Kubo formalism in accordance with the general scheme [5]. First we consider a sample with rectangular cross section of size $a \times b$; the layer thicknesses are c_j, with the layer index j=1 and 3 referring to two outer ferromagnetic parts and j=2 to a paramagnetic spacer.

The one-electron Green function $G^\sigma(x, y, z, x', y', z')$ ($0 < x, x' < a$, $0 < y, y' < b$) in coordinate-energy representation is the solution of the following equation:

$$\left(\Delta + \frac{2ME_j^\sigma}{\hbar^2}\right) G^\sigma = \frac{2Ma_0}{\hbar^2}\delta(\vec{r} - \vec{r'}), \tag{1}$$

obeying the continuity of G^σ and its derivatives at the interfaces between the layers; in addition we impose the condition $G^\sigma = 0$ on the outer (lateral) interfaces. Index σ denotes the spin projection of the electron. The complex value E_j^σ depends on the layer j; in case of a paramagnetic spacer one obtains

$$E_j^\sigma = \frac{2ME}{\hbar^2} + (k_{Fj}^\sigma)^2 + i\frac{2k_{Fj}^\sigma}{l_j^\sigma} \tag{2}$$

where E is the energy relative to the Fermi energy, l_j^σ is the mean free path and k_{Fj}^σ is the Fermi momentum of electrons with spin projection σ in the j-layer. The real part of the coherent potential is included in the Fermi energy. Both the d- and the s- electron Green functions obey equation (1) if the respective parameters are used. We suppose that the spin splitting of the s-band is negligibly small. The solution of Eq. (1) can be written in the form

$$G^\sigma(\vec{r}, \vec{r'}) = \sum_{n,m} \frac{4}{ab} G_{nm}^\sigma(z, z') \sin\frac{\pi n x}{a} \sin\frac{\pi m y}{b} \sin\frac{\pi n x'}{a} \sin\frac{\pi m y'}{b} \tag{3}$$

where $G_{nm}^\sigma(z, z')$ obeys the equation

$$\left(\frac{\partial^2}{\partial z^2} + \epsilon_{nm}^{\sigma(j)}\right) G_{nm}^\sigma(z, z') = \frac{2Ma_0}{\hbar^2}\delta(z - z') \tag{4}$$

with

$$\epsilon_{nm}^{\sigma(j)} = \frac{2ME_j^\sigma}{\hbar^2} - \left(\frac{\pi n}{a}\right)^2 - \left(\frac{\pi m}{b}\right)^2$$

Eq.(4) coincides with the equation for the Green function for infinite multilayers as obtained in [12], were also the solution of this equation has been

presented. Note that the values of the mean free path l_j^σ and the Fermi momentum k_{Fj}^σ depend on the size of the wire cross section; they can be calculated in the following way:

To renormalize the Fermi energy we equate the total (s and d) electron concentration $n = 2n_s + n_{d\uparrow} + n_{d\downarrow}$ for an infinite volume to the concentration of the electrons in a finite-size sample. Here n_s is the one-half concentration of s-electrons and $n_{d\sigma}$ is the concentration of d-electrons with spin σ. The electron concentrations are given by

$$n_{s,d\sigma} = -\mathrm{I}m\frac{1}{\pi}\frac{1}{abc}\int\limits_0^{E_F}\int G^\sigma(\vec{r},\vec{r},E)d^3rdE \tag{5}$$

.

The resulting k_{Fj}^σ values are then used to calculate the mean free path of the s-electrons:

$$\frac{l^\sigma(a,b,c)}{l^\sigma(a\to\infty,b\to\infty,c\to\infty)} = \frac{\rho_{d\sigma}(a,b,c)}{\rho_{d\sigma}(a\to\infty,b\to\infty,c\to\infty)}.$$

Note that both the density of states and the mean free paths of s-electrons oscillate with different periods as a function of nanowire cross section due to the different Fermi momenta of d-electrons with opposite spins.

The current perpendicular to the multilayer plane is given in the framework of the Kubo formalism as

$$J(z) = \frac{1}{\pi}\frac{e^2}{\hbar^2}\left(\frac{\hbar^2}{2M}\right)^2\int\sum_{n,m=1}^{\infty}\Bigg\{\Big[\frac{\partial G_{nm}^\sigma(z,z')}{\partial z} - \frac{\partial G_{nm}^{\sigma *}(z,z')}{\partial z}\Big]\Big[\frac{\partial G_{nm}^\sigma(z,z')}{\partial z'} - \frac{\partial G_{nm}^{\sigma *}(z,z')}{\partial z'}\Big] - \Big[\frac{\partial^2 G_{nm}^\sigma(z,z')}{\partial z\partial z'} - \frac{\partial^2 G_{nm}^{\sigma *}(z,z')}{\partial z'\partial z}\Big][G_{nm}^\sigma(z,z') - G_{nm}^{\sigma *}(z,z')]\Bigg\}E(z')dz' \tag{6}$$

As in the case of laterally infinite multilayers [5] we assume constant effective fields inside each layer to achieve nondivergence conditions for the current $\partial J(z)/\partial z = 0$; the total voltage across the length of the nanowire $U = \sum_{j=1}^3 \mathcal{E}_j c_j$, with $\mathcal{E}_j$ the effective field in the jth segment directed along the z-axis.

Next, the GMR can be calculated from the resistivities for parallel ($R(\uparrow\uparrow)$) and antiparallel ($R(\uparrow\downarrow)$) magnitizations of the ferromagnetic layers:

$$\frac{\Delta R}{R} = \frac{R(\uparrow\downarrow) - R(\uparrow\uparrow)}{\mathrm{m}in\{R(\uparrow\uparrow), R(\uparrow\downarrow)\}} \tag{7}$$

In addition, following the model described in ref. [15], we also calculated the tunneling magnetoresistance (TMR) of the nanowire if the paramagnetic spacer is replaced by an insulating spacer. In this case the spin-dependent resistance is due to the d-electron behavior since the exchange splitting of the d-band causes spin-dependent potential steps between the segments. Green functions obey the same *Eqs.* (1,2) with k^{σ}_{Fj} replaced by $-V_0$, where V_0 is height of the barrier. Denoting the real and imaginary parts of the electron momentum as k^{σ}_j and d^{σ}_j:

$$k^{\sigma}_j + id^{\sigma}_j = \sqrt{\epsilon^{\sigma(j)}_{nm}}$$

one obtains for $d_2c_2 \gg 1$ an expression for the conductivity of electrons with spin projection σ similar to $Eq.(3)$ of ref. [16] but with discrete momenta:

$$\Sigma^{\sigma} = \sum_{n,m} \frac{e^2}{\pi\hbar} \frac{16k^{\sigma}_1 k^{\sigma}_3 d_2^2 \exp(-2d_2c_2)}{((k^{\sigma}_1)^2 + (d_2 + d^{\sigma}_1)^2)((k^{\sigma}_3)^2 + (d_2 + d^{\sigma}_3)^2)}, \qquad (8)$$

where the $k's$ and $d's$ depend on the indices n, m, and $d_2 = \sqrt{V_0}$. In the general case (d_2c_2 not $\gg$1), this expression is much more complicated.

A few examples of our calculations are shown in Figs. 1-5 [17]. In Fig.1 the dependencies of the volume-averaged s- and d- electron DOS on the wire cross section size ($a = b$) are presented for Fermi momenta fixed at its value for $a = b \to \infty$ (Fig. 1a) as well as renormalized according to the procedure described above (Fig.1b). The curves show pronounced oscillations with periods equal to π/k^{σ}_{Fj}. The required renormalization of the Fermi energy leads to a noticeable change of the structure of the curves. The thin curve with large amplitude of oscillations describes the DOS of s-electrons in the paramagnetic spacer, whereas the the heavy curve with small amplitude describes the oscillations of the d-electron DOS in the ferromagnetic segments. The large amplitude of the oscillations in the spacer compared with the amplitude of oscillations in the ferromagnetics is due to the small thickness (c_2) of the spacer. The dependence of s-electron conductivity on the size a is defined by the oscillating behaviour of the mean free paths and DOS of s-electrons. These dependencies have to be considered as a complicated superposition of oscillating s and spin up and spin down d-electron's densities of states. They are shown in Fig. 2 for ferromagnetic and antiferromagnetic configurations. The parameters were chosen to reproduce the maximum experimental GMR for a CPP geometry at 4.2 K for $Co|Cu|Co$ multilayers [18].

Fig.3 shows the dependence of the GMR on the wire dimension a. As in Fig. 2, this curve is the superposition of several oscillating curves with different periods. In the maxima, the curve reaches much higher values than in case of $a = b \to \infty$, i.e., in a multilayer sample. To interprete this enhancement we have to take into account that the GMR is controlled by the spin polarization of the current which (for negligibly small thickness of the paramagnetic spacer) is proportional to the ratio $\left\{(l^{\uparrow} - l^{\downarrow})/(l^{\uparrow} + l^{\downarrow})\right\}^2$; since $l^{\uparrow}$ and $l^{\downarrow}$ oscillate with different periods this ratio oscillates as well and thus can produce high peaks, while for $k_F^{\uparrow} \approx k_F^{\downarrow}$ the GMR will be almost constant. As expected, the GMR oscillation becomes more pronounced for decreasing nanowire dimensions. This is in qualitative agreement with the experiment [19] in which GMR values between 40% and 200% were observed in few-atom sized nanocontacts at 4K. In these experiments the contact sizes were not controlled and vary statistically; therefore, the GMR values were statistically dispersed as well. It was observed, however, that the GMR is higher for samples with larger contact resistance, e.g. smaller dimension. This observation confirms our suggestion that the GMR can achieve high values in case of very thin wires, possibly of the order of several 100 % for dimensions in the range of a few Angstroms. We also note that for some specific Fermi momenta and mean free paths the calculated GMR changes sign in some region of cross section size (Fig.4).

The calculated TMR is represented in Fig.5 for different thicknesses of the insulating spacer. Firstly, we note that the absolute value of the TMR as well as the form of the curves strongly depend on the thickness of the spacer. Secondly, the oscillation amplitude as a function of size a is much smaller if compared with the GMR oscillations in a nanowire of the same size. The reason is that due to the exponential factor (see Eq. (8)) the conductivity is mainly determined by the term with minimal $d_2 c_2$ ($n = m = 1$).

Finally, we want to point out that the resistivities and the GMR have been calculated for ideal outer interfaces and specular reflection of the electrons. A roughness of the interfaces can lead to a smoothing of the oscillations. This effect will be addressed in a future publication.

A. V. Vedyayev acknowledges the CENG DRMC SP2M for hospitality and the Russian Foundation of Fundamental Research for financial support. M. Ye. Zhuravlev is grateful to Bielefeld University for hospitality. The work has been supported by the Deutsche Forschungsgemeinschaft in the

"Forschergruppe Nanometer-Schichtsysteme".

References

[1] M.N. Baibich, Phys. Rev. Lett. **61** (1988) 2472; G. Binasch, Phys. Rev. **B39** (1989) 4828.

[2] Special Issue: J. of Magentism and Magnetic Materials, Vol. 200, No. 1-3 (1999).

[3] T. Valet and A. Fert, Phys. Rev. **B 48** (1993) 7099;

[4] P. M. Levy, S. Zhang and A. Fert, Phys. Rev. Lett **65** (1990) 1643 H. E. Camblong, P. M. Levy and S. Zhang, Phys. Rev. **B 51** (1995) 16052

[5] A. Vedyayev, N. Ryzhanova, B. Dieny, P. Dauguet, P. Gandit , J. Chaussy, Phys. Rev. **B 55** (1997) 3728

[6] H. E. Camblong, S. Zhang and P. M. Levy, Phys. Rev. **B 47** (1993) 4735

[7] K. M. Schep, P. J. Kelly, and G. E. W. Bauer, Phys. Rev. **B 57**, (1998) 8907

[8] W. H. Butler, X. G. Zhang, D. M. C. Nicholson, and J. M. Maclaren, Phys. Rev. **B 52** (1995) 13399

[9] E. Yu. Tsymbal and D. G. Pettifor, Phys. Rev. **B 54** (1996) 15314

[10] M. D. Stiles, J. Appl. Phys. **79** (1996) 5805

[11] J. Mathon, Phys. Rev. **B 55** (1997) 960

[12] A. Vedyayev, C. Cowache, N. Ryzhanova and B. Dieny, J. Phys.: Condens. Matter **5** (1993) 8289

[13] A. Fert and I. A. Campbell, J. Phys. F: Met., **6** (1976) 849

[14] F. Brouers, A. Vedyayev, and M. Giorgino, Phys. Rev. **B 7** (1973) 380

[15] A. Vedyayev, N. Ryzhanova, C. Lacroix, L. Giacomoni and B. Dieny, Europhys. Lett. **39** (1997) 219

[16] A. M. Bratkovsky, Phys. Rev. **B 56** (1997) 2344

[17] In the calculations we supposed that the Fermi momenta in both ferromagnetics depend only on the spin projection of the electron relative to the magnetization. Therefore, we use two parameters $k_F^{\uparrow,\downarrow}$ for the Fermi momenta of d-electrons with direction of spin parallel and antiparallel to the magnetization, and k_F^s for the Fermi momenta of s-electrons in all three segments. For simplicity we suppose that the Fermi momentum of d-electrons in the paramagnetic segment equals to k_F^s as well. The same notations are held for the mean free paths of d-electrons. The bulk values of the corresponding Fermi momenta and the mean free paths are given in the figure captions.

[18] W.P. Pratt, Jr., S.-F. Lee, J. M. Slaughter, R. Loloee, P. A. Schroeder, and J. Bass, Phys. Rev. Lett, **66** (1991) 3060;
P. Holody, W. C. Chiany, R. Loloee, J. Bass, W.P. Pratt, Jr., and P. A. Schroeder, Phys. Rev. **B 58** (1998) 12230

[19] N. García, M. Muñoz, Y.-W. Zhao, Phys. Rev. Lett. **82** (1999) 2923

Figure captions

Fig.1a,b.
Normalized DOS of s-electrons in the paramagnetic spacer (thin line) and d-electrons in the ferromagnetic segment (heavy line) with fixed bulk Fermi momentum (1a) and renormalized Fermi momentum (1b). $k_F^{\uparrow}$=1.40 Å^{-1}, $k_F^{\downarrow}$=0.40 Å^{-1}, k_F^{s}=1.20 Å^{-1}; $l^{\uparrow}$=15.0 Å, $l^{\downarrow}$=120.0 Å, l_2=215.0 Å; $c_1 = c_3$=22.0 Å, c_2=7.0 Å. Here $\uparrow$ refers to electrons with spin parallel to magnetization, $\downarrow$ refers to electrons with spin antiparallel to magnetization and s refers to electrons in the paramagnetic spacer. c_j is the thickness of the corresponding layer j.

Fig.2.
The normalized resistivity for parallel magnetization, $R(\uparrow\uparrow)$ (solid line) and antiparallel magnetization, $R(\uparrow\downarrow)$ (dotted line) for $k_F^{\uparrow}$=1.40 Å^{-1}, $k_F^{\downarrow}$=0.40 Å^{-1}, k_F^{s}=1.20 Å^{-1}; $l^{\uparrow}$=15.0 Å, $l^{\downarrow}$=120.0 Å, l_2=215.0 Å; $c_1 = c_3$=22.0 Å, c_2=7.0 Å.

Fig.3a,b.
GMR for the parameters used in Fig.1

Fig.4.
GMR for $k_F^{\uparrow}$=0.87 Å^{-1}, $k_F^{\downarrow}$=0.60 Å^{-1}, k_F^{s}=1.19 Å^{-1}; $l^{\uparrow}$=67.02 Å, $l^{\downarrow}$=120.02 Å, l_2=215.02 Å; c_1=22.8 Å, c_3=23.2 Å, c_2=7.3 Å.

Fig.5a,b.
TMR for $k_F^{\uparrow}$=1.40 Å^{-1}, $k_F^{\downarrow}$=0.40 Å^{-1}, V_0=1.44 Å^{-2}; $l^{\uparrow}$=21.0 Å, $l^{\downarrow}$=100.0 Å; the thickness of the ferromagnetic segments $c_1 = c_3$ = 23.0 Å, the thickness of the insulator spacer c_2 = 4.0 Å(a) and 20.0 Å(b).

Fig. 1a.

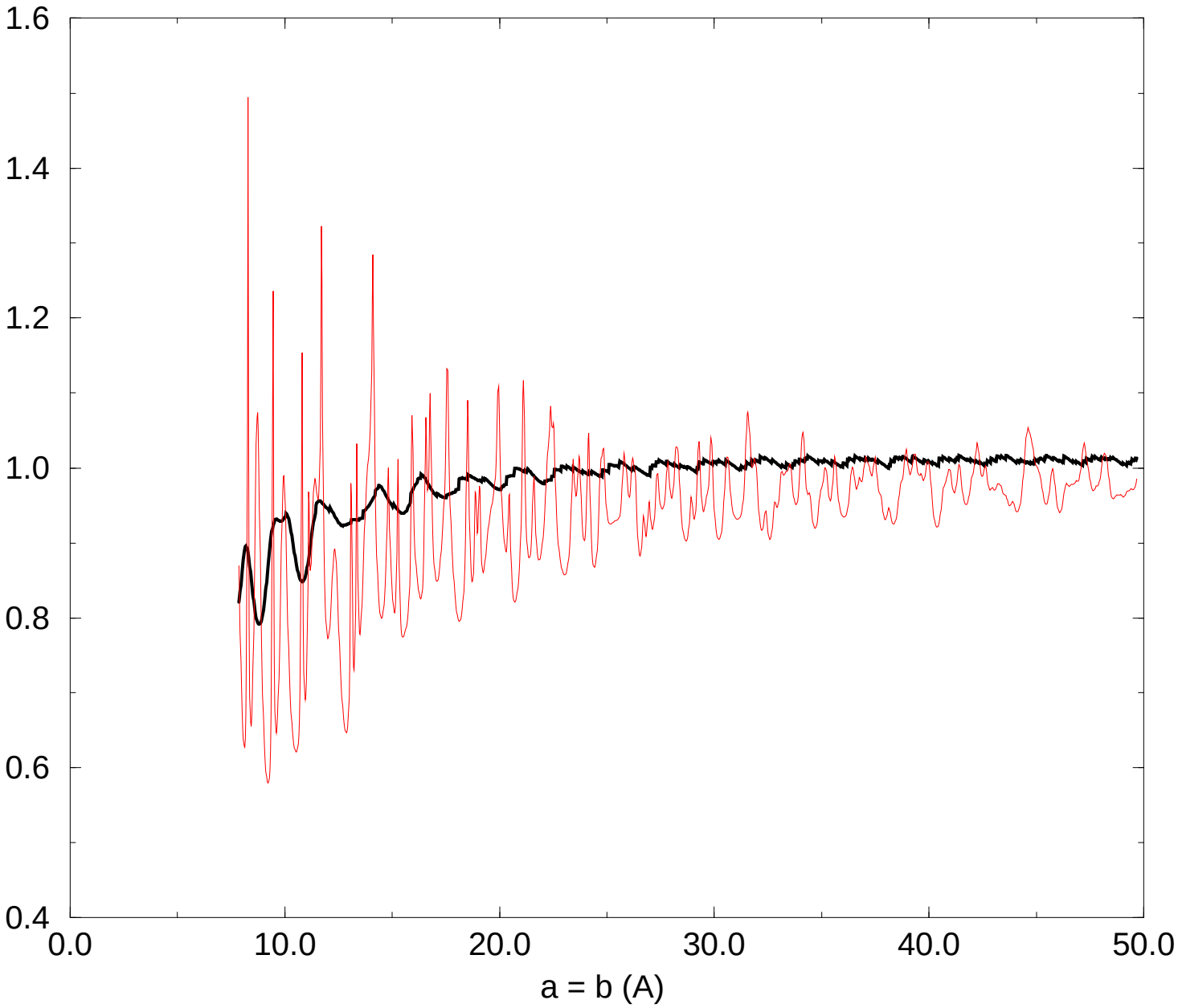


Fig. 1b.

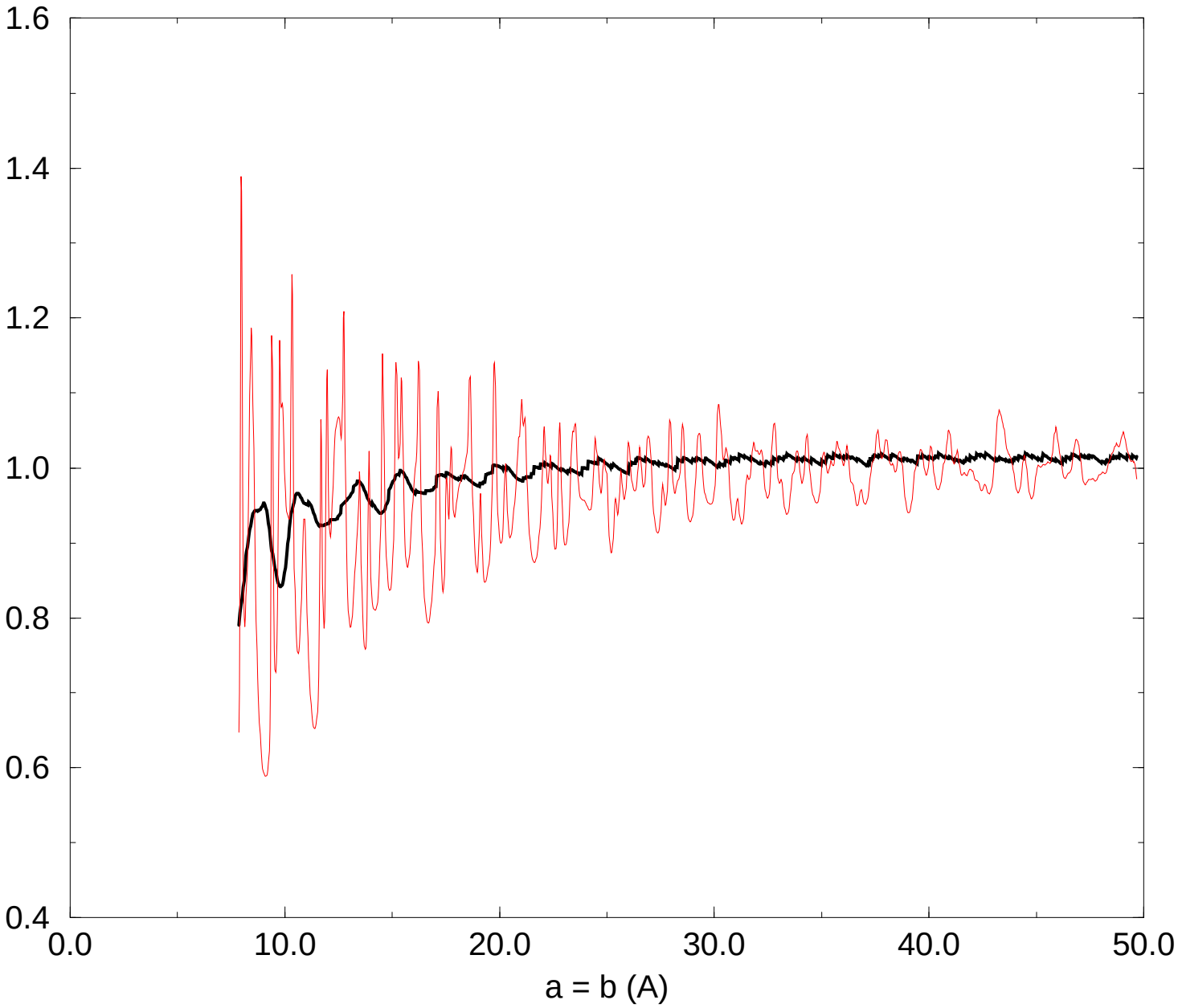


Fig. 2.

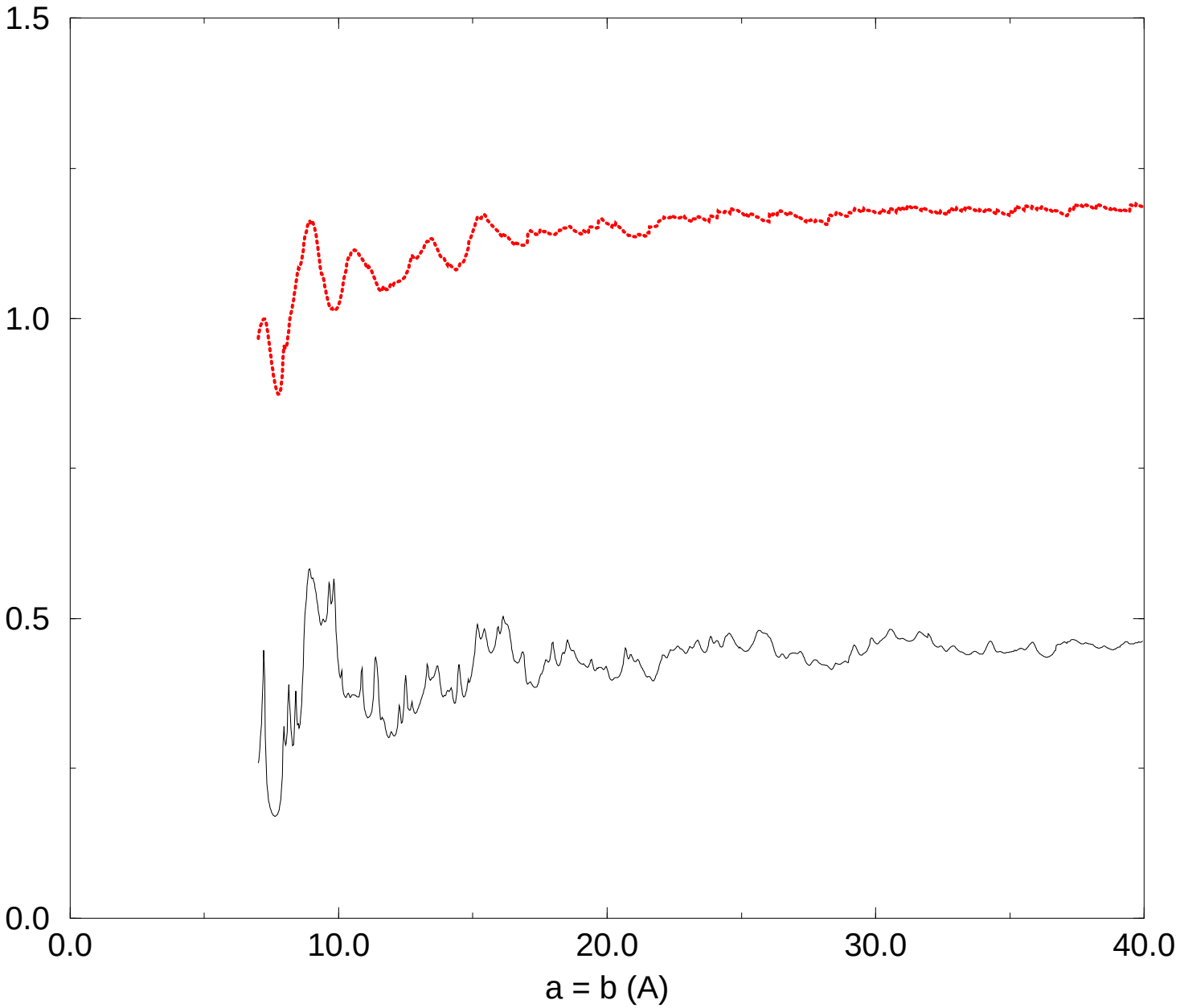


Fig. 3a

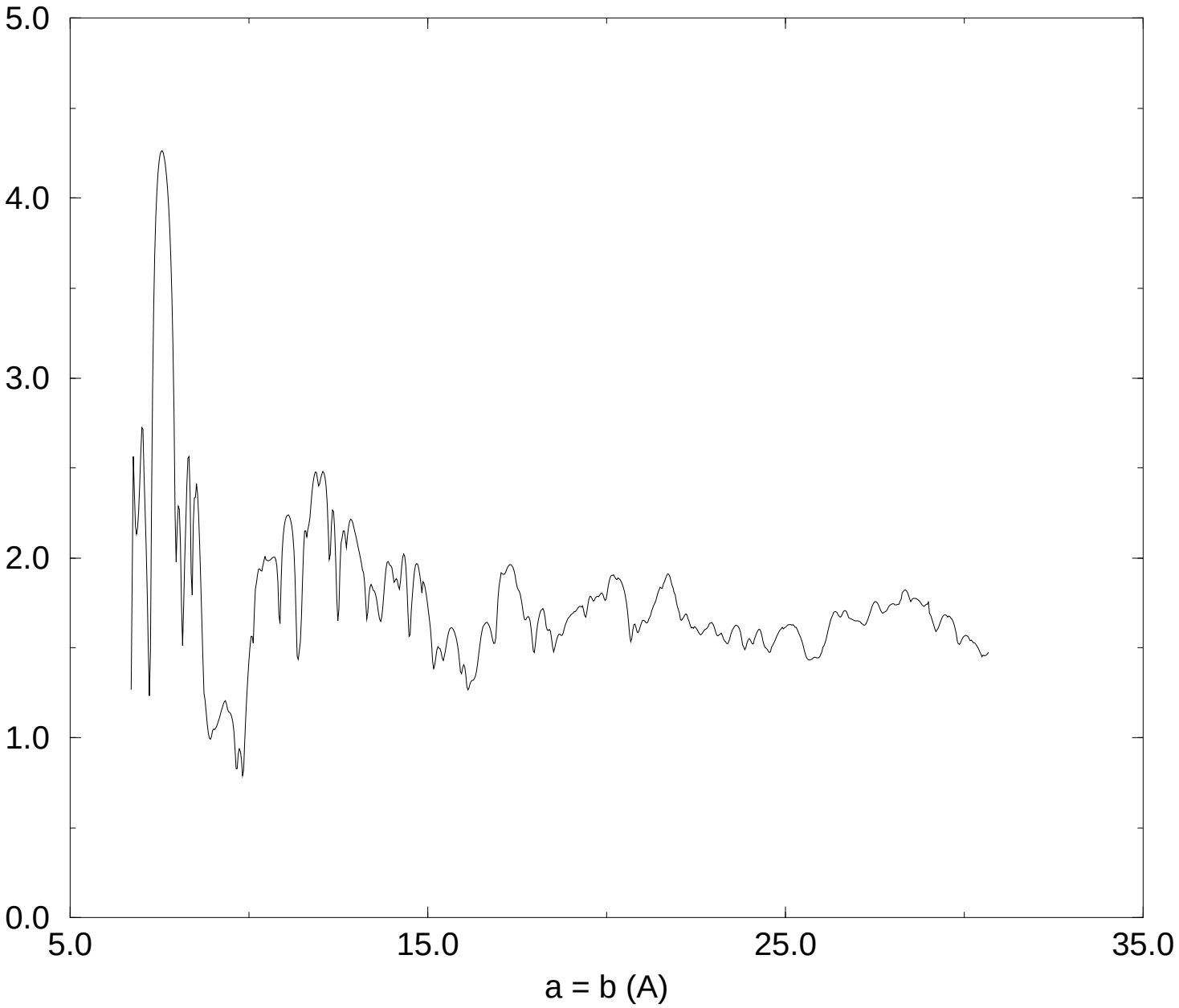


Fig. 3b

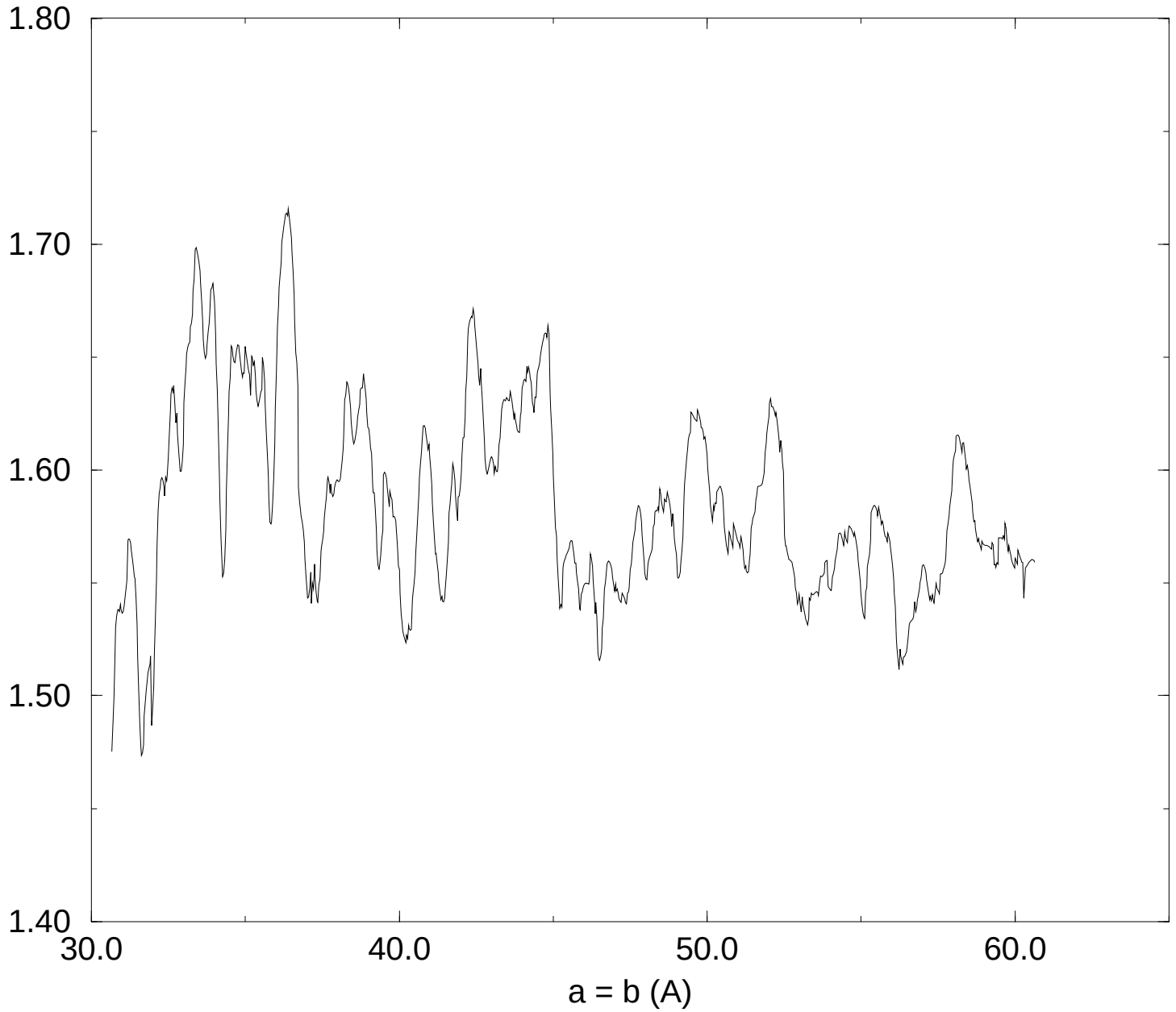


Fig. 4.

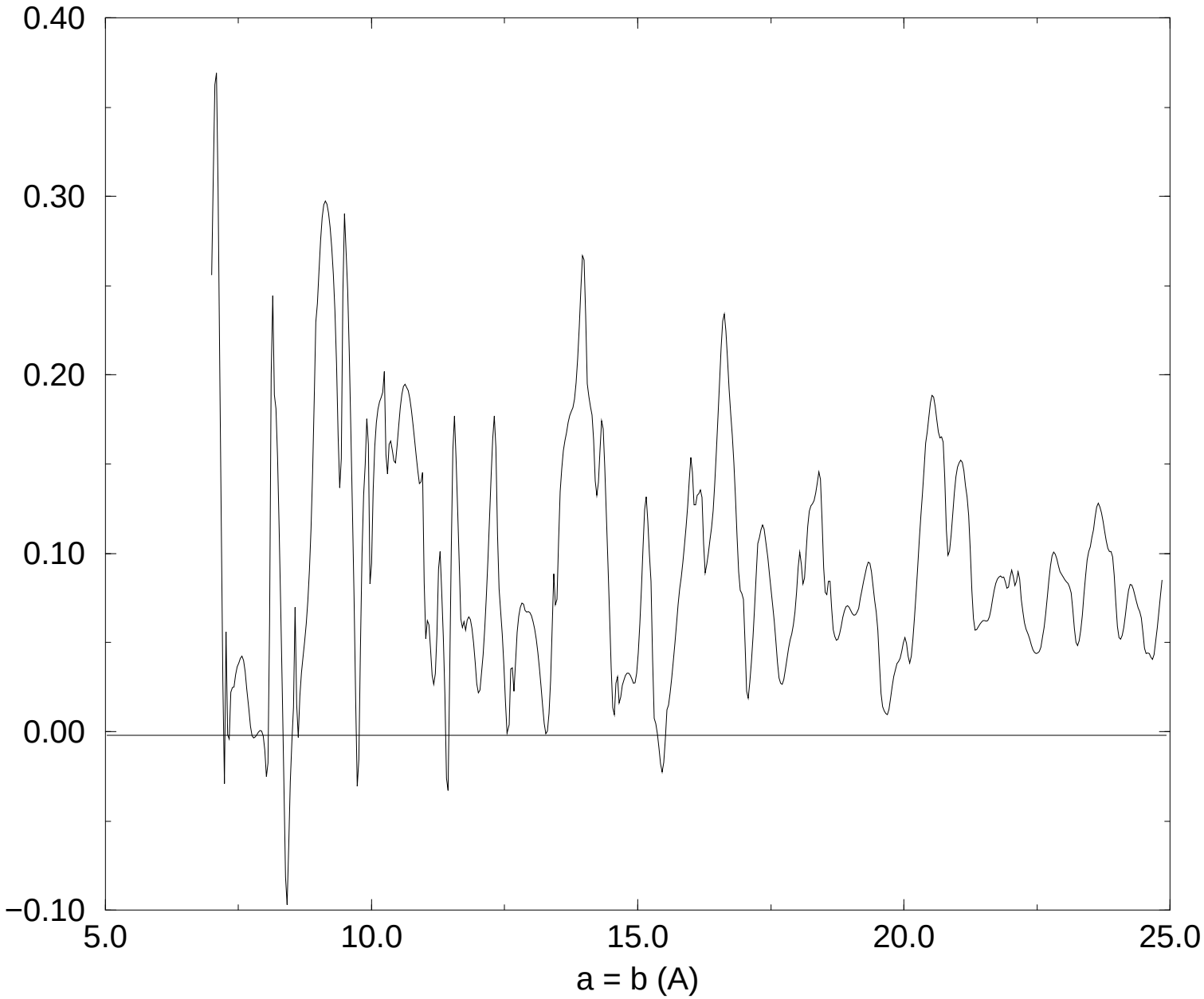


Fig. 5a.

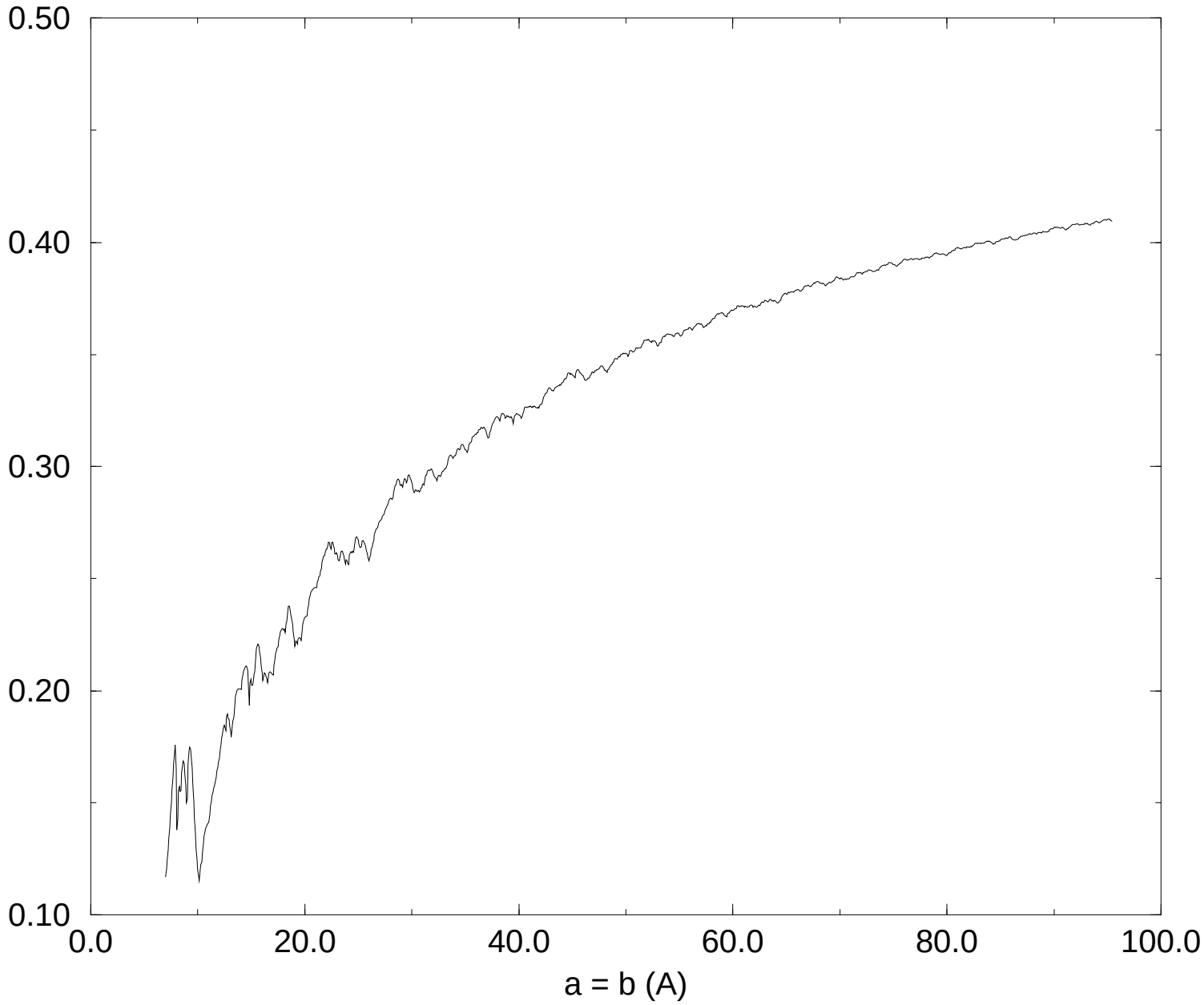


Fig. 5b.

